Modeling and Experiments of Untethered Quadrupedal Running with a Bounding Gait: The Scout II Robot[1]

Ioannis Poulakakis[2], James A. Smith[2] and Martin Buehler[3]
poulakas|jasmith@cim.mcgill.ca, buehler@BostonDynamics.com

[2]Ambulatory Robotics Laboratory, http://www.cim.mcgill.ca/~arlweb
Department of Mechanical Engineering and Centre for Intelligent Machines
McGill University
3480 University Street
Montreal, QC H3A 2A7, Canada

[3]Boston Dynamics
515 Massachusetts Avenue
Cambridge, MA 02139, U.S.A.

Submitted to the International Journal of Robotics Research as a Full Paper
December 2003, Revised September 2004, Accepted October 2004

[1] Portions of this paper have been previously appeared in [38] and [30]. The third author was an Associate Professor at McGill University and the Director of the Ambulatory Robotics Lab when this work was performed.

ABSTRACT

This paper compares models and experiments involving Scout II, an untethered four-legged running robot with only one actuator per compliant leg. Scout II achieves dynamically stable running of up to 1.3 m/s on flat ground via a bounding gait. Energetics analysis reveals a highly efficient system with a specific resistance of only 1.4. The running controller requires no task-level or body-state feedback and relies on the passive dynamics of the mechanical system. These results contribute to the increasing evidence that apparently complex dynamically dexterous tasks may be controlled via simple control laws. The authors discuss general modeling issues for dynamically stable legged robots. Two simulation models are compared with experimental data to test the validity of common simplifying assumptions. The need for including motor saturation and non-rigid torque transmission characteristics in simulation models is demonstrated. Similar issues are likely to be important in other dynamically stable legged robots as well. An extensive suite of experimental results documents the robot's performance and the proposed models' validity.

KEY WORDS – Legged locomotion, modeling, quadrupedal robot, dynamic running, bounding gait, dynamic stability.

1. INTRODUCTION

As mobile robots are required to operate outside the laboratory, the limitations of traditional wheeled and tracked vehicle designs become increasingly apparent. To overcome these limitations, one branch of the mobile robotics field has turned to biological inspiration for other possible solutions, including *legged* systems, which promise a versatility and mobility unparalleled in more traditional designs.

Early attempts to implement legged designs resulted in slow moving, statically stable systems. These designs are still the most prevalent today. One of the more successful examples of this large class of legged robots is Hirose's Titan series [16]. Because of the negligible momentum in the gaits developed by such vehicles, maintaining stability requires only that the position of the Center-Of-Mass (COM) is kept within the polygon of support created by the stance legs [36].

In this paper we focus on dynamically stable legged robots. To date, the most significant research on dynamic legged locomotion was led by Raibert at the CMU and MIT Leglabs in the 1980s and 1990s [32]. His research revolved around fundamental principles for controlling hopping height, forward speed and body posture, making various gaits possible on monopedal, bipedal and quadrupedal robots. His controllers resulted in fast and stable dynamic running with different paired-leg gaits, such as the trot, pace and bound.

Other dynamically stable running designs have been proposed since Raibert, including the articulated-knee Scamper bounding quadruped by Furusho et al. [12]. The controller divided one running cycle into eight states and switched the two joints per leg between free rotation, position control and velocity control. Following a different approach, Kimura et al. implemented bounding by transitioning from pronking in the Patrush robot based on principles from neurobiology [17]. They combined explicit compliance with a neural oscillator network, whose frequency matched that of the vertical spring-mass environment-system oscillation. Patrush's three Degree-Of-Freedom (DOF) legs each featured an actuated hip and knee, and an unactuated, compliant foot joint while the robot was physically constrained to move in the sagittal plane by overhead beams. Other leg designs have also been proposed, most involving more actuators than Scout II. One such recent design is the OSU-Stanford KOLT quadrupedal robot that houses all of the leg actuators at the hip or on the body [25].

Various models have been proposed to study dynamically stable quadrupeds. Murphy and Raibert studied bounding and pronking using a model with kneed legs whose lengths were controllable [31]. They discovered that active attitude control in bounding is not necessary when the body's moment of inertia is smaller than the mass times the square of the hip spacing. Following-up on their work, Berkemeier showed that this result applies to a simple linearized running-in-place model and that it can also be extended to pronking [4]. Brown and Raibert investigated the conditions for obtaining passive cyclic motion [31]. They studied two limiting cases of system behavior: the grounded and the flight regimes, and found that the system in both regimes can passively trot, gallop or bound if provided with the proper initial conditions. More recently, from a minimalist open loop perspective and inspired by results in biomechanics [19], and dynamical systems [14], Poulakakis et al. showed that passively generated stable bounding of a conservative model of Scout II is possible under appropriate initial conditions and sufficiently high speeds [27], [28].

In a different spirit, Formalsky et al. investigated ballistic motions of a sagittal quadrupedal model involving leg pairs such as the trot, the pace and the bound that were achieved by appropriate initial speeds resulting from impulsive active control torques acting at the boundaries of support phases [9]. Other work on modeling the dynamics of quadrupedal running includes studies of more complex gaits such as galloping, where no legs are used in pairs. Schmiedeler and Waldron studied the kinematics and dynamics of the gallop on a three-dimensional, five DOF quadruped with massless legs, where they found that as drag increases, the footfall patterns approach the half-bound gait [34]. Herr and McMahon studied the transverse gallop of a horse-type model and concluded that their robot model could exhibit stable galloping without requiring control over postural orientation and also without any sensing of body attitude [15].

This paper addresses a subject that is central to advancing the state of the art in autonomous, dynamically stable legged locomotion beyond the purely experimental realm: *experimentally validated models*. Although many models for open or closed loop dynamic legged locomotion have been studied (e.g. [4], [9], [15], [31], [34]), and many simulation techniques have been proposed for efficient integration of the dynamic equations and visualization of the resulting motion (e.g. [10]), *no* models exist in the literature which are experimentally validated down to the actuator torque level. And yet, without such validation, the relevance of theoretical and simulation results to physical legged robots remains uncertain. Thus, we turn our attention to proposing (Section 4) and testing (Section 5) various modeling assumptions for Scout II. Power autonomous legged robots like Scout II typically operate at the limits of their actuators and require a model of the actuator dynamics and their interaction with the power source. Furthermore a detailed description of the hip torque transmission systems, including belt compliance and gearbox dynamics, is necessary for achieving more accurate simulations.

Before deriving models and studying their experimental validation, we introduce the subject of our study in Section 2: the Scout II quadrupedal robot [5] (Fig. 1). Scout II features a radically new, and indeed simplest, mechanical design of any dynamically stable running quadruped to date: it has only one actuator per leg located at the hip, which actively rotates the leg in the sagittal plane while the leg itself has a single prismatic compliant joint. In Section 3 we introduce a simple controller, which demonstrates experimentally that dynamic running on flat

ground via a bounding gait is possible by merely positioning the legs at a fixed desired touchdown angle during flight (not modified during successive strides), and commanding a motor torque during stance until a sweep limit angle is reached. The most striking feature of the controller is that it *only* requires touchdown/lift-off detection and local feedback of the leg angles relative to the body, available from leg potentiometers and motor encoders respectively, which, are the *only* sensors needed. The motion is largely the result of the interaction between the actuators and the *natural* dynamics of the mechanical system. To the best of the authors' knowledge, Scout II is the first power and computationally autonomous quadrupedal robot that achieves compliant running *and* features the simplest running control algorithm.

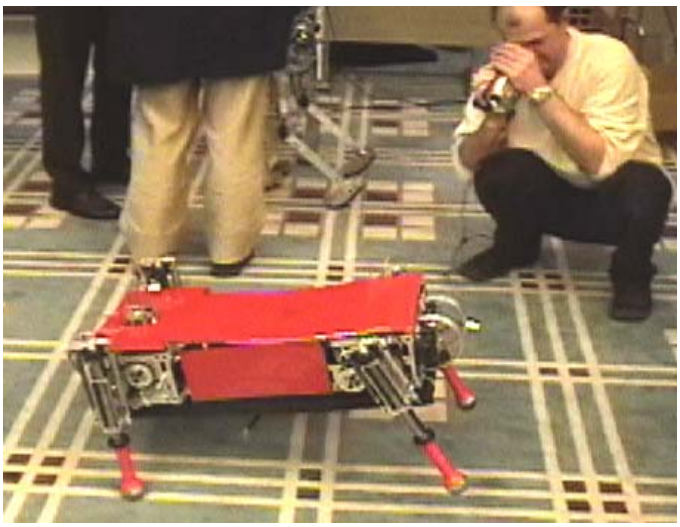

Figure 1. Scout II running during a demonstration at AMAM2003 in Kyoto, Japan [29].

The fundamental contribution of Scout II is the demonstration that fast and stable dynamic quadrupedal locomotion can be achieved without a high power leg actuator, directly changing the energy stored in the compliant legs during stance. Beyond the fundamental insights into the control and dynamics of legged locomotion, the practical implications are significant. With reliability and cost being some of the main obstacles to the commercial viability of legged robots, mechanical simplicity is essential. A Scout II–like robot has potential applications in education or entertainment. If rough terrain mobility is desired, the legs could be rotated full circle to achieve optimal ground clearance. In fact, this idea, while not implemented in Scout II, in part gave rise to the design of the six-legged, highly mobile RHex robot [33]. RHex uses the same single-actuator-per-compliant-leg principle as its precursor, Scout II [5]. Finally, if full leg

revolution is not desired, a low power knee actuator (locked during stance) can be added, which merely reduces the leg length during the flight phase for improved ground clearance, resulting in greatly improved rough terrain mobility.

2. MECHANICAL DESIGN AND EXPERIMENTAL PLATFORM

2.1. Design Concept

The design of Scout II (Fig. 2, refer to [3] for details) is an exercise in simplicity. It consists of a rigid body with four compliant prismatic legs. The most striking feature of Scout II is the fact that it uses only a *single* actuator per leg located at the hip joint, which provides leg rotation in the sagittal plane. Each leg assembly consists of a lower and an upper leg, connected via a spring to form a compliant prismatic joint. Thus each leg has two DOF: the hip's rotational DOF (actuated), and the prismatic compliant DOF (passive).

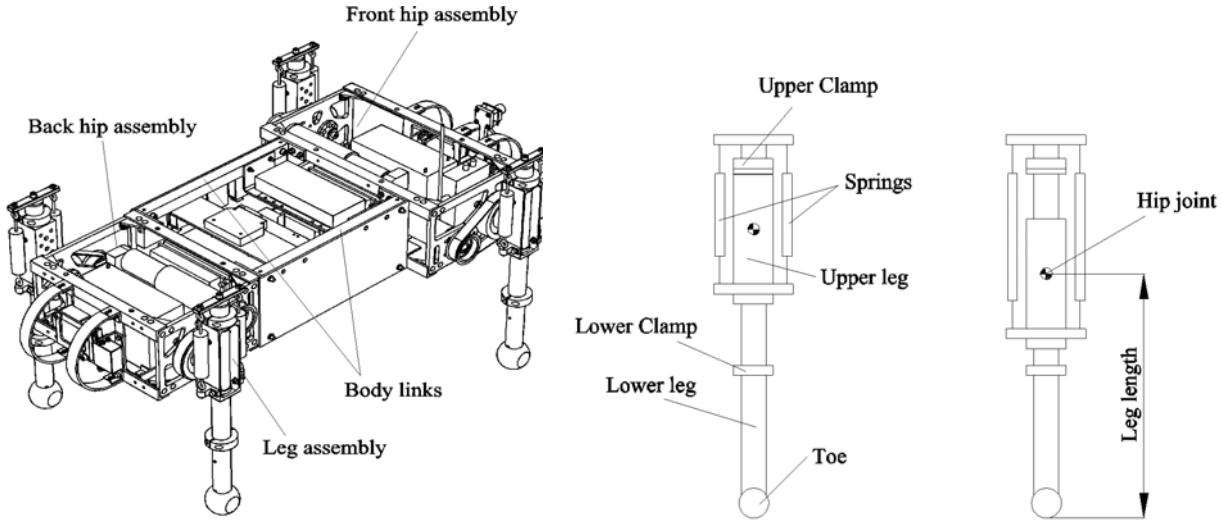

Figure 2. Mechanical structure of Scout II (left) and compliant prismatic leg design with one actuated hip DOF (right). Figures adapted from [3], [37].

This configuration allows for the realization of different dynamically stable running gaits on flat ground such as dynamic walking [8], pronking [37], bounding [26], [38], as well as dynamic step climbing [37]. Furthermore, half-bounding and galloping have recently been implemented for the first time [29]. In this paper however, we concentrate on the bounding running behavior both in simulation and in experiments.

2.2. Hardware Description

The chassis of Scout II (see Fig. 2) consists of three modules: one torso and two hip assemblies. The torso forms a structure that houses the computer unit with the I/O boards as well as one of the three batteries. The front and back hip assemblies house two batteries and the actuation mechanisms including amplifiers, motors, gearboxes and pulleys.

Each hip is actuated by a Maxon 118777 brushed DC motor, a Maxon 110404 three-stage planetary gearbox [21], and a belt and pulley pair, which further amplifies the torque and isolates impact forces from the motor shaft. The motor position and thus the leg angles are controlled via 1 kHz Proportional-Derivative (PD) control loops. The motors are driven by four Advanced Motion Controls 25A8 PWM servo amplifiers [1]. The amplifiers control the current to the motor, thus delivering predictable torques at the motor shaft as long as the motors are not saturated. The system operates at 36 V nominal voltage, provided by three battery packs, each consisting of ten Sanyo HR-D NiMH cells. Scout II has a PC/104 stack with a 300 MHz Pentium II class processor, which, together with multiple I/O boards, collects data from the sensors and performs all the necessary computations for implementing the various controllers.

Various sensors are used to monitor the motion of Scout II. Apart from incremental optical encoders that measure the angular displacements of the motor shafts, linear potentiometers measure leg lengths, and are *only* used to infer ground contact. Laser range finders are used to measure the distance of the front and back ends of the robot from the ground and thus provide an estimate of the body's pitch and COM height.

2.3. Scout II Bounding Model

In this paper, we restrict our attention to the bounding running gait. The essentials of the motion in bounding take place in the sagittal plane and the motion is assumed to be planar. Therefore, Scout II can be considered as a three-body kinematic chain composed of the body and the front and back leg pairs, also called the *virtual* legs [32] (see Fig. 3). A linear spring/damper system models the leg compliance during the stance phase.

Each of the virtual legs can be in stance or in flight resulting in four *robot states*: double leg flight, back leg stance, double leg stance and front leg stance. In each of these phases the equations of motion of the system are different, placing Scout II in the category of *intermittent* or

variable structure systems. The two-dimensional model presented in Fig. 3, can be described by seven coordinates

$$\mathbf{x} = \begin{bmatrix} x & y & \theta & \varphi_b & l_b & \varphi_f & l_f \end{bmatrix}^T, \tag{1}$$

where all the variables and the sign conventions are shown in Fig. 3 and are summarized in Table I. The design parameters of the robot are presented in Table II. Note that an alternative representation of the system's configuration would be to express the leg angles relative to the vertical i.e.,

$$\gamma_i = \varphi_i + \theta, \tag{2}$$

where $i = b, f$.

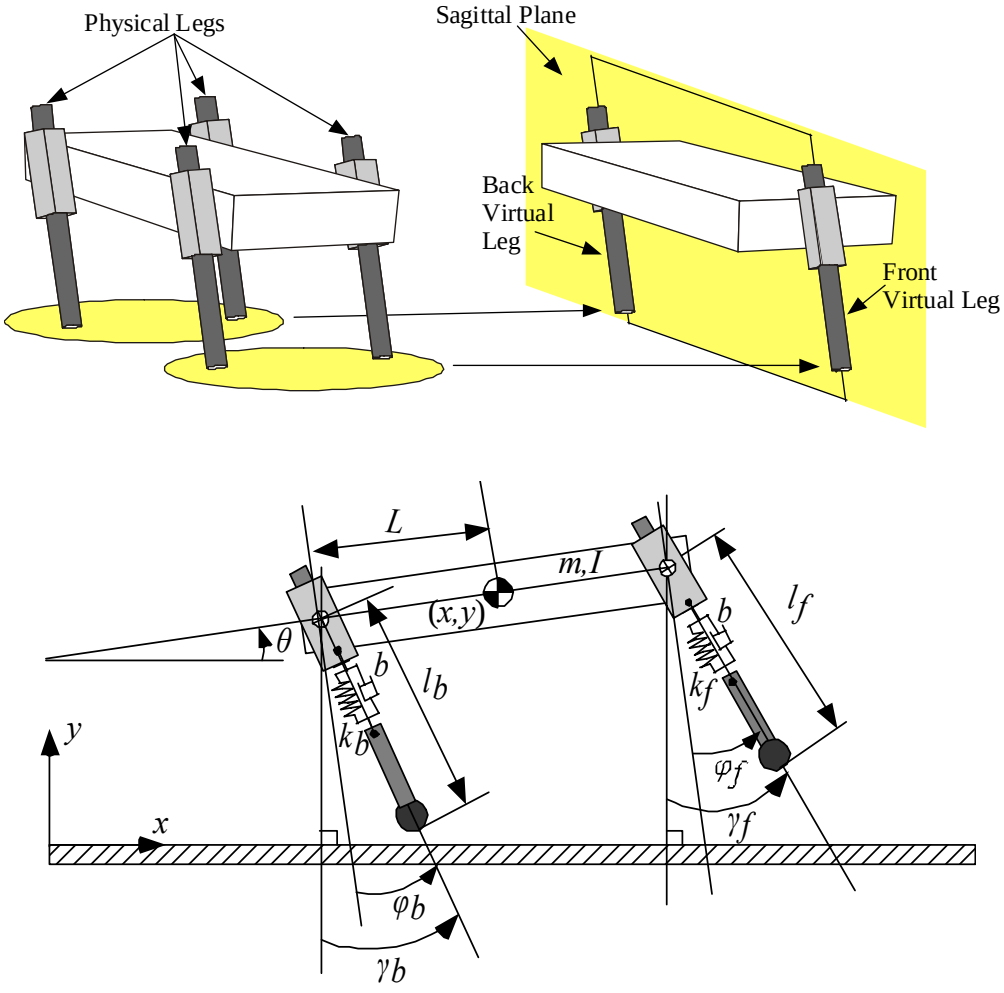

Figure 3. Virtual legs for the bounding gait and the two-dimensional bounding model for Scout II in the sagittal plane.

Table I. Scout II Variables

Symbol	Description
(x, y)	COM Cartesian coordinates
θ	Pitch angle
φ_i	Leg angle relative to the body
γ_i	Leg angle relative to the vertical
l_i	Leg length

Table II. Scout II Parameters

Symbol	Description
L	Half hip spacing
l_0	Nominal leg length
m	Body mass
I	Body moment of inertia
k_i	Spring stiffness, i^{th} leg
b_i	Damping constant, i^{th} leg

3. BOUNDING CONTROLLERS

3.1. Constant Touchdown Angle Bounding Controller

The controller proposed in this paper can be parameterized by four parameters φ^{td}, φ^{swl}, A, $\tau_{\max}$, representing the touchdown and sweep limit angles, the motor torque/speed slope and its maximum torque, respectively, for each of the virtual legs. The controller is structured in two hierarchical levels. At the high level the control action independently regulates the motion of the front and back virtual legs based on their state, without a notion of overall body state. The front and back virtual legs each detect three possible *leg states*: stance-retraction, stance-brake and flight, which are separated by touchdown, sweep limit and lift-off events, as shown in Fig. 4. There is no actively controlled coupling between the front and back virtual legs - the bounding motion is purely the result of the controller interaction through the multi-body dynamic system. At the low level, the controller ensures that the assumptions for the virtual legs hold true so that the front and back physical legs are properly synchronized to form the front and back virtual legs, respectively. This leg synchronization function changes the desired torque value to each leg in the lateral leg pair using a PD controller which monitors hip angle and angular velocities, ensuring that the corresponding error is small. To enforce the virtual leg assumption, state changes only occur when both physical legs in a lateral pair have the same state, a requirement that can be relaxed to allow for three-dimensional gaits [29].

Depending on the state of the virtual legs, different control actions are assigned by the high level controller as shown in Fig. 5.

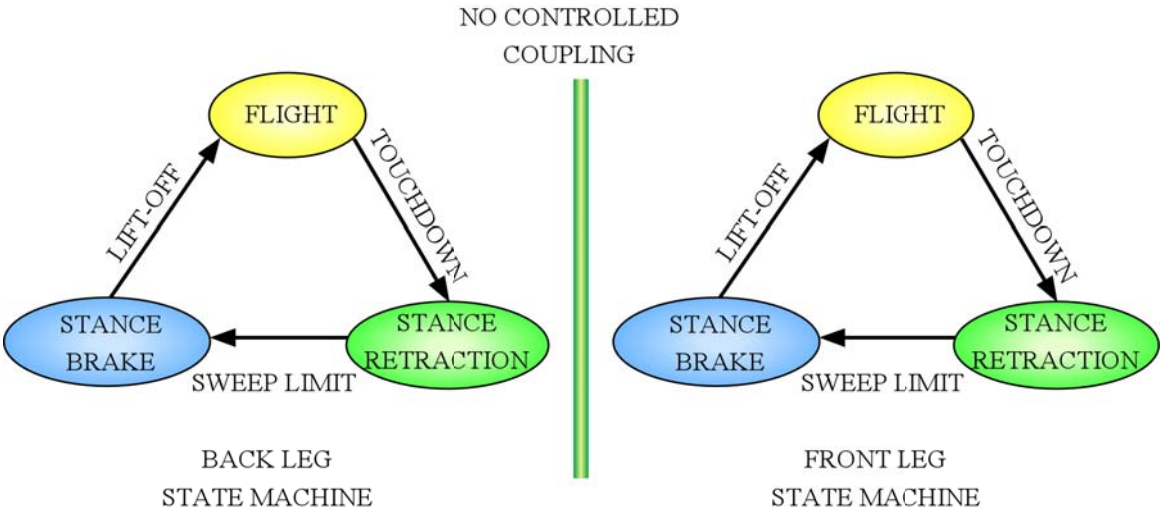

Figure 4. The bounding controller state machine.

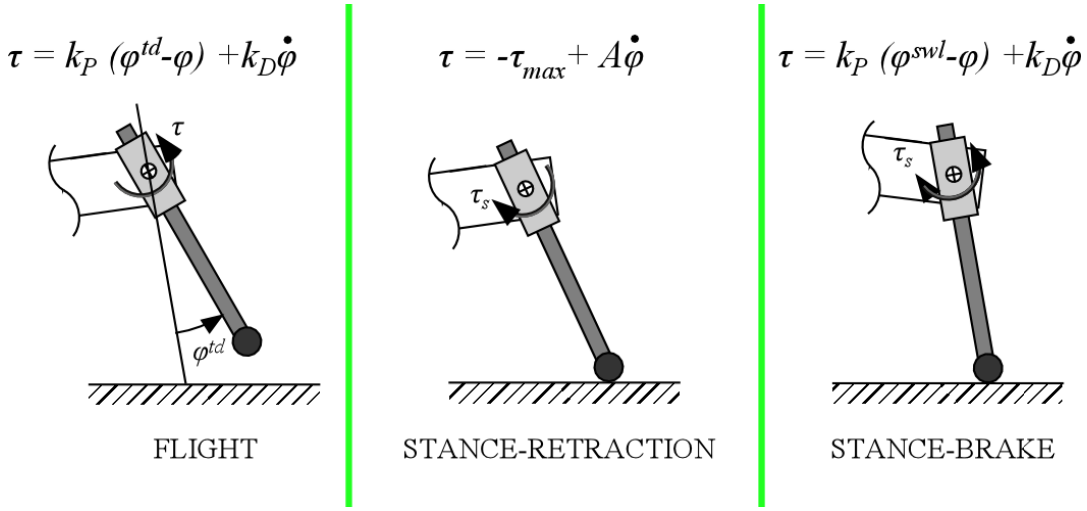

Figure 5. Control action during the phases of the bounding gait.

Flight. During the flight leg state, the controller servos the leg to a desired touchdown angle φ^{td}, which is defined with respect to the body, resulting in the φ*-controller*. Variations of the flight controller can be introduced by defining the touchdown angles with respect to the vertical, resulting in the γ*-controller* (see [37]). However, as opposed to the φ-controller, the γ-controller requires body-state feedback, namely the pitch angle θ, which is necessary for calculating γ from (2). Because we follow a minimalist approach in this paper, we have included only φ-controller results. It is important to mention here that recent work [27], [28], reveals the significance of the touchdown angles as inputs directly available for the control of

Scout II's cyclic motion. This fact, in combination with the actuator saturation constraints during the stance phase, suggests that the leg touchdown angles, rather than the actuator torques, are the *dominant* control inputs during cyclic motion. Therefore, *most* of the control action is applied during flight (for a theoretical justification in the context of the Spring Loaded Inverted Pendulum (SLIP) template see [2]).

Stance-Retraction. During this leg state, the controller sweeps the leg backwards, until a sweep limit angle φ^{swl} is reached. Actuator constraints are the dominant feature in the stance-retraction phase. The motors have to be capable of not only supporting the robot's weight, but also of imparting significant accelerations to the body, and to support large dynamic loads. Therefore, they often operate at their limits, characterized by their torque/speed curve. While this curve is well known, it is rarely taken into account in robot modeling and control. To include motor saturation in our controller, we command torques according to

$$\tau_{\text{des}} = -\tau_{\max} + A\dot{\varphi} \tag{3}$$

$$\tau_{\max} = \alpha \frac{K_T \bar{V}}{R_A},\ A = -\beta \frac{K_T K_\omega}{R_A}, \tag{4}$$

where $\tau_{\max}$ and A are the offset and the slope of the torque/speed line referred at the leg and $\dot{\varphi}$ is the leg's rotational speed. In (4) K_T and K_ω are the torque and speed constants of the motor respectively and R_A is its armature resistance. The values of these parameters are available in [21] and are presented in Table III. The parameters α and β in (4) are used to relate variables at the motor shaft (prior to the gearbox) to the corresponding ones at the leg (after the gearbox) and are given by

$$\alpha = \left[\left(n_G \eta_G\right)\left(n_P \eta_P\right)\right],\ \beta = \left[\left(n_G^2 \eta_G\right)\left(n_P^2 \eta_P\right)\right], \tag{5}$$

where n_G and η_G correspond to the ratio and the efficiency of the gearbox and n_P and η_P to the pulley combination and efficiency respectively; see Table III.

In (4), $\bar{V}$ represents the average voltage at the motor terminals, which is set to $36\ \text{V}$. Note also that according to our sign conventions, during stance-retraction the motors operate in the third quadrant where both the torque and speed are negative. There are two additional constraints that must be imposed on the desired hip torques τ_{des},

$$\text{if } |\tau_{des}| > \alpha K_T \, i_{\max} \text{ then } \tau_{des} = -\alpha K_T \, i_{\max}, \tag{6}$$

$$\text{if } \tau_{des} \geq 0 \text{ then } \tau_{des} = 0. \tag{7}$$

The constraint (6) ensures that the commanded torque will not exceed the maximum value predicted by the amplifier current limit $i_{\max}$, which is discussed in Section 4.1. The constraint (7) prevents the commanded torque from becoming positive, thus decelerating the robot[2].

Table III. Motor Parameters

Parameter	Value	Units
Torque Constant	0.0389	Nm/A
Speed Constant	6.78×10^{-4}	V/deg/s
Armature Resistance	1.23	Ω
Belt & Pulley Combination	48/34	n/a
Belt & Pulley Efficiency	96%	n/a
Planetary Gear Ratio	72.38	n/a
Max. Gear Efficiency	68%	n/a

Stance-Brake. When the sweep limit event is reached (when the leg angle becomes smaller than a specific sweep limit angle φ^{swl}), a PD controller holds the leg at that angle. Although, this modification has the undesirable effect of braking the robot, it is necessary for ensuring toe clearance especially during the early protraction phase because of the absence of active control of the leg length during flight. The addition of the sweep limit was found to significantly improve the robustness of the motion at the expense of performance and energy consumption.

It is important to mention that the controllers described here are simpler than those proposed by Raibert in two respects. First, *no* task-level (e.g. forward velocity) and *no* body-state (e.g. body posture) feedback is required and second, *no* explicit control over leg length ensuring toe clearance during the leg protraction phase is necessary, provided that the modification outlined above is added to the stance phase. These characteristics have had and are expected to have significant implications in the design of other legged robots too. Indeed, similar design and

[2] (6) arises when $\dot{\varphi}$ is too small so that excessively large torques are predicted from (3) which cannot be applied by the motors due to saturation of the PWM amplifiers that are not capable of delivering sufficiently large currents. (7) occurs when the legs spin at speeds large enough to result in a sign change of the desired torque.

control ideas have been successfully used to generate bounding in the modified (one actuator per leg) AIBO [39], and by Campbell and Buehler [7] in the hexapedal RHex, developed by Buehler and Koditschek and their collaborators [33].

3.2. The Resulting Bounding Gait

Fig. 6 presents snapshots of the robot's motion along with experimental data showing cyclic motion. The controller parameters used for each of the physical legs are presented in Table IV and the resulting average forward speed was 1.3 m/s.

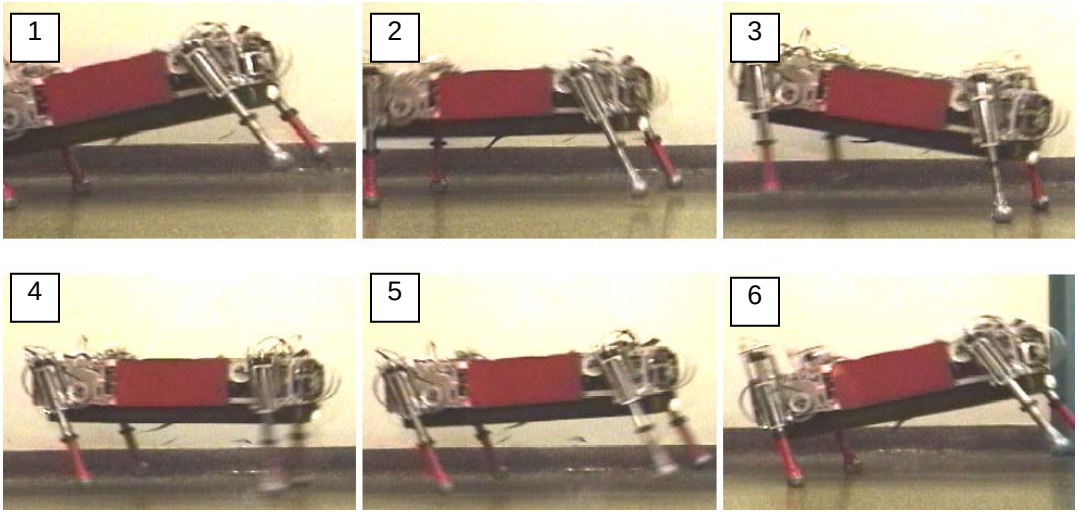

Table IV. Controller parameters
(SI units, angles in degrees)

Parameter	Front	Back
Touchdown Angle	21	19
Sweep Limit Angle	0	0
Flight (k_P, k_D)	(250,5)	(250,5)
Stance-brake (k_P, k_D)	(300,5)	(300,5)

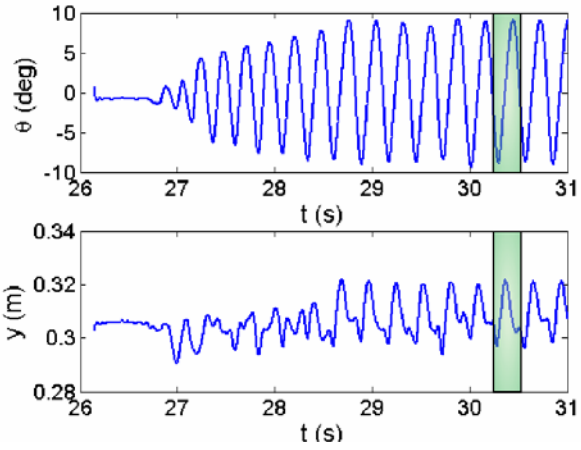

Figure 6. Snapshots of the robot at different phases (top) and body pitch and hopping height data (bottom right) in the bounding gait implemented on Scout II.

It should be mentioned here that, based on the control strategy presented in Section 3.1, a family of similar controllers can be introduced by changing the control action during the flight

(e.g. control the leg angle γ relative to the vertical instead of the φ angle) or the stance phase (e.g. control the sweep speed $\dot{\varphi}$). As was shown in [37] these significant controller differences have relatively minor effects on bounding performance. Moreover, variations of the φ-controller recently resulted in the half-bound and rotary gallop gaits for the first time [29].

3.3. Energetics

For mobile robots to be of practical utility, they must operate in a power autonomous fashion for extended periods of time. An increasingly accepted measure of energy efficiency is the *specific resistance* - a measure originally proposed by Gabrielli and von Karman [13],

$$\varepsilon(\upsilon) = \frac{P(\upsilon)}{mg\upsilon}, \tag{8}$$

where P is the power expenditure, m is the mass of the vehicle, g is the gravitational acceleration constant, and υ is the vehicle speed.

Since many vehicle specific resistances quoted in the literature are based on the average mechanical output power of the actuators, we illustrate this as a function of speed in Fig. 7. Even though energy efficiency has not been optimized, Scout II at top speed achieves a low specific resistance based on mechanical power, equal to 0.47. This value places Scout II among the most energy efficient running robots, only slightly higher than the (lowest published running robot efficiency) 0.22 value for the ARL Monopod II [6], but still lower than any other running robot.

The specific resistance based on mechanical output power has drawbacks, since it does not take the actuator efficiency or the power consumption of the entire system into account. Both of these effects can have a dramatic negative influence on runtime. Therefore, a more useful measure of energy efficiency is the specific resistance based on total power consumption. For Scout II, the specific resistance based on electrical power[3] is approximately 1.4 at a forward speed of about 1.3 m/s, i.e. three times the specific resistance based on mechanical power. As can be seen in Fig. 7, at an average speed of approximately 0.85 m/s the specific resistance related to mechanical output is approximately 0.75 while the electrical specific resistance is approximately 2.2, indicating that Scout II becomes less efficient at lower speeds. For this reason we concentrate on higher speeds in this paper. For reasons of comparison, Fig. 7 (right) also

[3] The electrical power is calculated as the total average product of battery current and voltage.

includes the specific resistance based on electrical power published in [7] for RHex in bounding and pronking.

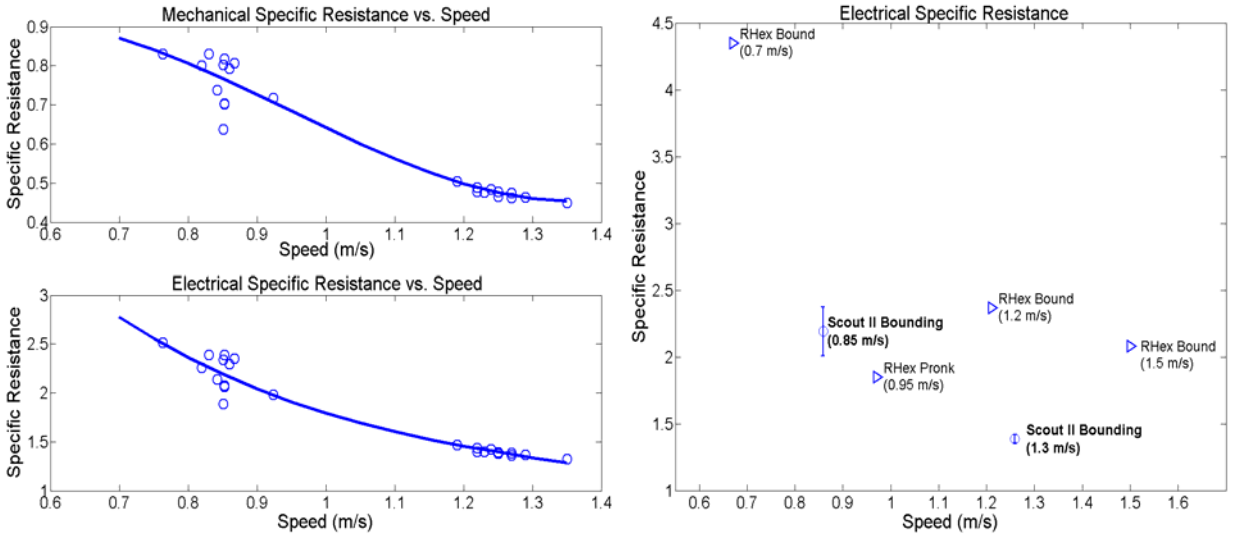

Figure 7. Specific resistance for Scout II based on mechanical and electrical power (left) and specific resistance based on electrical power for Scout II and RHex [7]. Error bars indicate standard deviation.

3.4. Discussion

Scout II is a highly nonlinear, underactuated, intermittent dynamical system. Furthermore, as Full and Koditschek state in [11] p. 3326, “Locomotion results from complex, high-dimensional, nonlinear, dynamically coupled interactions between an organism and its environment.” Thus, the task itself is also complex and cannot be specified via reference trajectories in Cartesian or in state space. Even if such trajectories could be found, developing a tracking controller is still not straightforward or perhaps even possible. Friction, actuator limitations and unilateral ground forces limit the hip torques, which may be required to achieve trajectory tracking. Furthermore, there are no experimentally validated models, which could be used to derive model-based controllers for legged robots. This reveals the necessity for constructing simulation models to test the validity of various simplifying modeling assumptions as will be discussed in Section 5.

It is apparent from the above discussion why direct application of modern robot control theory had limited success in deriving controllers for dynamically stable legged robots. Despite this complexity, we found that simple Raibert-style control laws like those described in Section

3.1 and in [32], operating mostly in a feedforward fashion, with minimal sensing, can stabilize periodic motions resulting in robust and fast running powered by only four hip actuators. It is therefore natural to ask why such a complex system can accomplish such a complex task via minor control action.

As outlined in [27] and [28], a possible answer is that Scout II's unactuated, conservative dynamics *already* exhibit *asymptotically stable* bounding cycles and therefore a simple controller is all that is needed to keep the robot bounding. Indeed, for sufficiently high forward speeds and pitch rates there exists a regime where the system can be *passively* stable and can tolerate small perturbations of the nominal conditions *without* any control action taken. This fact could provide a possible explanation as to why the Scout II robot can bound without the need for complex state feedback. It is important to mention that this hypothesis is in agreement with recent research in biomechanics, which shows that when animals run at high speeds, passive dynamic self-stabilization from a feed-forward, tuned mechanical system can reject rapid perturbations and simplify control [11], [19]. Analogous behavior has been discovered by McGeer in his passive bipedal running work [22], and more recently in the conservative[4] SLIP template [14], [35].

To conclude, Scout II and its simple, body-state and task-level open loop controller embodies these general underlying principles and can be considered as an experimental demonstration contributing to the increasing evidence that, as Full and Koditschek suggested in [11], control laws operating mostly in the feedforward regime with “mechanical feedback” are sufficient to induce stable dynamic behaviors in legged machines.

4. MODELING COMPONENTS

4.1. Electrical Subsystem

In this section we present simple models for the motor driving system, including the battery, PWM amplifier, actuator and gearbox units. As will be shown in Section 5, these models must be included in simulations to improve their accuracy. A battery-amplifier-motor combination actuating the front and back virtual legs may be approximated as shown in Fig. 8. We assume that the coupling between the lateral (physical) legs forming the front and back pairs is

[4] An explanation as to why conservative intermittent dynamical systems can exhibit asymptotically stable limit cycles despite the incompressibility of the stance flow was presented in [2].

insignificant so instead of modeling the four motors driving the actual legs, we model the two equivalent *virtual* motors actuating the front and back virtual legs.

Battery Model. Since electrically actuated autonomous robots draw significant peak power and operate from non-ideal voltage sources, the variation of the supply voltage as a function of the total load current must be considered. As shown in Fig. 8, the battery model is composed of a resistance, R_b, in series with an ideal voltage source, V_{nom}. The equation that describes the output voltage is,

$$V_b = V_{nom} - i_b R_b . \tag{9}$$

To determine the parameters in (9), namely V_{nom} and R_b, the current i_b and voltage V_b were measured during a set of experiments and then the model described by (9) was fit in a least square sense to the experimental data resulting in the values $V_{nom} = 37.17$ V and $R_b = 0.13\ \Omega$. As can be seen from Fig. 9 (left), the simple battery model described by (9) captures the resulting supply voltage fluctuations occurring in experiments.

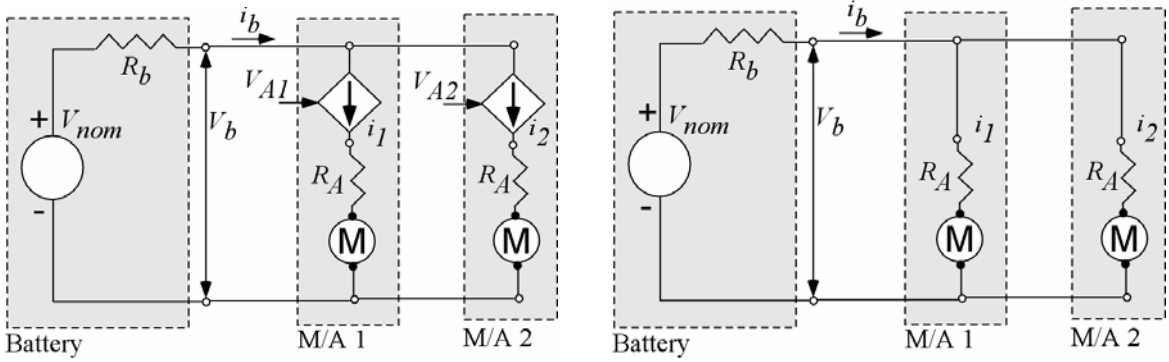

Figure 8. Two motor/amplifier blocks in parallel with the battery: Amplifiers operate in current mode (left) and motors operate in saturation mode (right).

Motor/Amplifier Model. As was mentioned above, actuator constraints are dominant in Scout II's motion and ignoring them not only results in a large discrepancy between simulation and experimental data but, most importantly, may also result in failure of the simulation model to converge to stable cyclic bounding motion. Fig. 8 shows the model for the amplifier/motor combination when the amplifier is in current and in saturation modes.

We assume that the PWM switching signal may be completely removed from the motor input. When the motor is not saturated, the amplifier operates in current mode and achieves the

desired motor current by appropriately adjusting its terminal voltage via an internal current monitoring feedback loop [1]. In this regime, the amplifier can be approximated by an ideal voltage-controlled current source whose output current is directly proportional to its input voltage signal, denoted in Fig. 8 by V_{A1} and V_{A2}, i.e.

$$i_i = \frac{\tau_i}{K_T} = K_{amp} V_{Ai}, \tag{10}$$

where $i = 1, 2$ for the back and front virtual leg respectively and $K_{amp} = 4.3$ A/V is the voltage-to-current gain of the amplifier. Note that the amplifier's peak current is limited to $i_{\max} = 20$ A by internal circuitry to prevent the motor from being critically overdriven. This limit is taken into account in the stance-retraction controller by (6).

As the motor shaft accelerates under a desired torque $K_T i_{des}$, its rotational speed ω, increases until the back EMF $K_\omega \omega$, becomes larger than the available power supply voltage $V_b - i_{des} R_A$. Therefore, the current mode applies only up to a speed limit, $\omega_{\max}$, given by

$$\omega_{\max}\left(i_{des}\right) = \frac{V_b - i_{des} R_A}{K_\omega}, \tag{11}$$

after which the motor enters its saturation regime, where we assume that the amplifier operates as an ideal conductor, see Fig. 8 (right). In this regime the motor torque τ is given by

$$\tau = \frac{K_T}{R_A}\left(V_b - K_\omega \omega\right), \tag{12}$$

in which the motor inductance has been neglected. Combining (10) and (12) we obtain the equation describing the torque τ applied by the motor in both the saturation and non-saturation regimes. The leg torque $\hat{\tau}_{leg}$ that takes into account the motor but not the amplifier saturation can be calculated by the motor torque using

$$\hat{\tau}_{leg} = \begin{cases} -\alpha K_T i_{des} & \text{for } |\omega| \le |\omega_{\max}| \\ -\alpha \dfrac{K_T V_b}{R_A} - \beta \dfrac{K_T K_\omega}{R_A} \dot{\varphi} & \text{for } |\omega| > |\omega_{\max}| \end{cases}, \tag{13}$$

which is valid in the third quadrant of the torque/speed line (stance-retraction). In (13) the velocity $\omega_{\max}$ is given by (11), the parameters α and β are given by (5), and the sign

conventions described in Section 2.3 have been applied. Finally, the torque τ_{leg} that is delivered at the leg and that includes both the motor and amplifier saturation is given by

$$\tau_{leg} = \mathrm{sgn}\left(\hat{\tau}_{leg}\right) \ \min\left\{\left|\hat{\tau}_{leg}\right|,\ \alpha K_T i_{\max}\right\} \tag{14}$$

where $i_{\max}$ is the amplifier's peak current. Equations (13), (14) constitute the motor model in the third quadrant and with the appropriate sign changes can be extended to the first quadrant of the torque/speed curve.

Fig. 9 shows current, voltage and torque plots. The data curves in the right-hand plot of Fig. 9 are as follows, from bottom to top. The bottommost solid curve represents the desired torque from the controller as calculated by (3), which is identical to the one predicted by (14) for a fixed 36 V supply voltage. The second, dashed, curve is the maximum achievable torque and includes the battery voltage fluctuations calculated by (9). The third, dotted, curve illustrates the torque with an additional loop gain fix due to amplifier gain modeling error. Finally, the topmost solid curve represents the current-estimated motor torque measured during a bounding experiment. The exceptionally good match between the topmost solid and dotted torque curves in the right-hand plot of Fig. 9 validates the model and demonstrates both its importance and its effectiveness in predicting motor saturation.

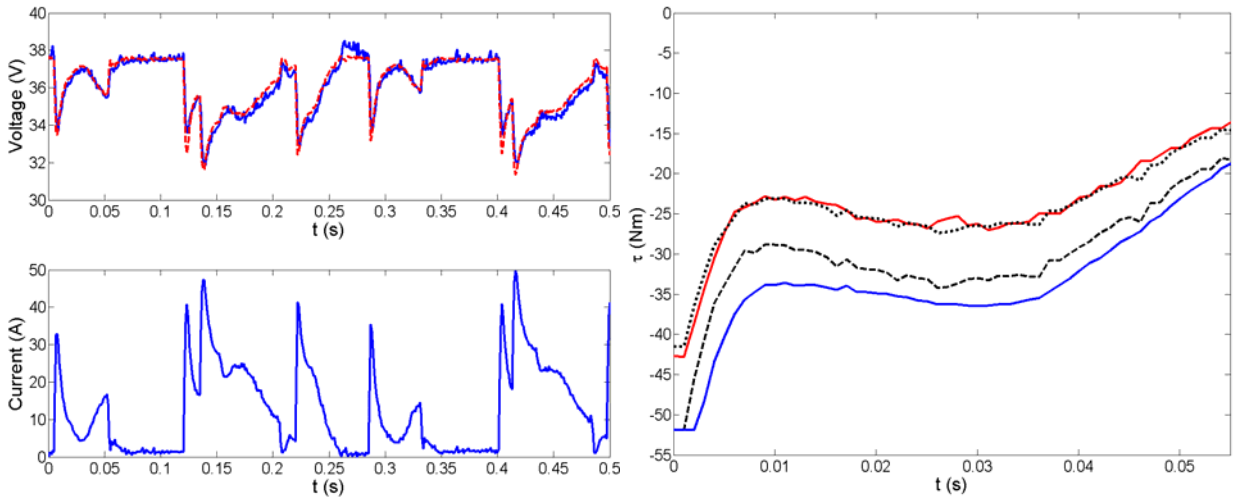

Figure 9. Left: Voltage (upper) and current (lower) measured in the experiment (solid lines) and voltage calculated (dashed line) using (9). Right: Torque profiles during the stance-retraction phase.

4.2. Mechanical Subsystem

Throughout the course of this research it has become clear that modeling only the motor driving system (batteries, PWM amplifiers and actuators) as in Section 4.1 is *not* sufficient for obtaining simulation results which closely follow the experimental data. A more detailed model of the hip unit that includes backlash and belt compliance, must be included in simulation in order to improve its accuracy. It is important to mention here that the assumptions of zero backlash and rigid torque transmission are very common in modeling dynamically stable robots. However, as will be shown in Section 5, for Scout II and the controllers presented in Section 3, they not only result in large mismatches between simulation and experimental data but more importantly, for some set points, they might even result in failure to converge to cyclic motion. Note also that these effects are not specific to Scout II. Indeed, because of space limitations for motor placement and due to the desire to isolate impact forces from the motor shafts, structural elements like belts are very common for torque transmission in leg designs e.g. [12]. Moreover, torsional compliance is inherent in composite leg designs as in RHex [23], even without the existence of belts. Therefore, the consequences of torsional compliance on the dynamics of the Scout II are likely to be significant in other dynamically stable robots.

To capture these effects, the three stage planetary gearbox has been approximated by a pair of spur gears as shown in Fig. 10, with a gear ratio equal to the combined gear ratios of the gearbox and pulleys. Also, friction and damping present in the hip joint were taken into account to improve the leg response during the flight phase. To estimate the values of the inertias of the drive and driven gears and the friction and damping coefficients of the hip joint, two sets of experiments were performed. In the first set a known mass was placed at the toe, the leg was brought to a known angle and then it was left to rotate freely. In the second set, the robot was placed so that both the front and back legs were in flight and various touchdown angles were commanded. All these experiments were simulated in Working Model 2D™ [18], and the resulting parameter values for the physical legs are presented in Table V.

Finally, the combined effect of gear backlash and belt compliance has been approximated by a rotational spring in parallel with a damper as shown in Fig. 10. The values of the hip spring/damper constants were chosen so that the maximum spring deflection during bounding in simulation does not exceed that which is measured by the robot applying maximum hip torque

with the torso and legs constrained on a horizontal plane (approximately 8^o of combined backlash and belt stretching).

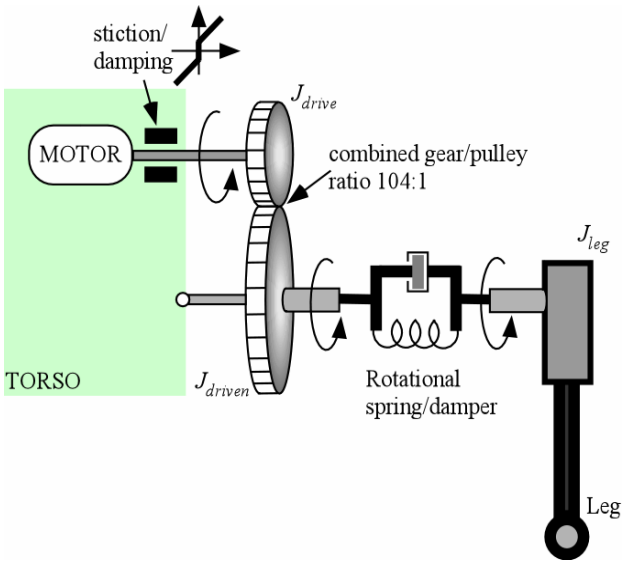

Table V. Hip Joint Properties

Parameter	Value	Units
Drive Gear Inertia	3.5×10^{-6}	kg m^2
Driven Gear Inertia	10^{-3}	kg m^2
Stiction (joint)	5.5×10^{-3}	Nm
Damping (joint)	6.2×10^{-7}	Nm/deg/s
Spring (belt)	7.0	Nm/deg
Damper (belt)	4.0	Nm/deg/s

Figure 10. Details and modeling parameters of the hip unit.

In all of the above experiments none of the structural elements were examined in isolation. For instance, isolating the gearbox and performing detailed identification experiments to find the inertia of the gears requires special equipment not available to the authors. Instead, we performed simple experiments examining the behavior of the hip unit as a whole under different dynamic conditions as described above. Then parameter values were selected that matched experiment and simulation under these different conditions.

5. EXPERIMENTS AND SIMULATION

5.1. Simulation Models

The planar model of Scout II, see Fig. 11, was constructed in Working Model 2D™ [18], to study the behavior of the robot using various controllers. This model, augmented with the motor driving system described in the previous sections, proved to be invaluable in deriving controllers which, when applied to our physical prototype, resulted in high performance robust running behaviors. The Working Model 2D™ script used to implement the controllers has the following structure. First, the model of the robot is generated, then the simulation loop collects the values

of the data of interest (i.e. the values of the state variables of the robot), by integrating the dynamic equations and, based on these values, calculates the desired torques. The desired torques are entered into a subroutine, which implements the motor driving system described in Section 4.1 and returns the actual torques that form the inputs to the hip "actuator constraints". The animation step is set to 1 ms, which matches the control loop time step used on the Scout II robot, and which can be different from the integration step. The adaptive step Kutta-Merson integrator was used with integration error set to 1e-10, to obtain the simulation results. Two models were used to test the validity of simplifying modeling assumptions common to the literature. These models, whose parameters are listed in Table VI, are illustrated in Fig. 11.

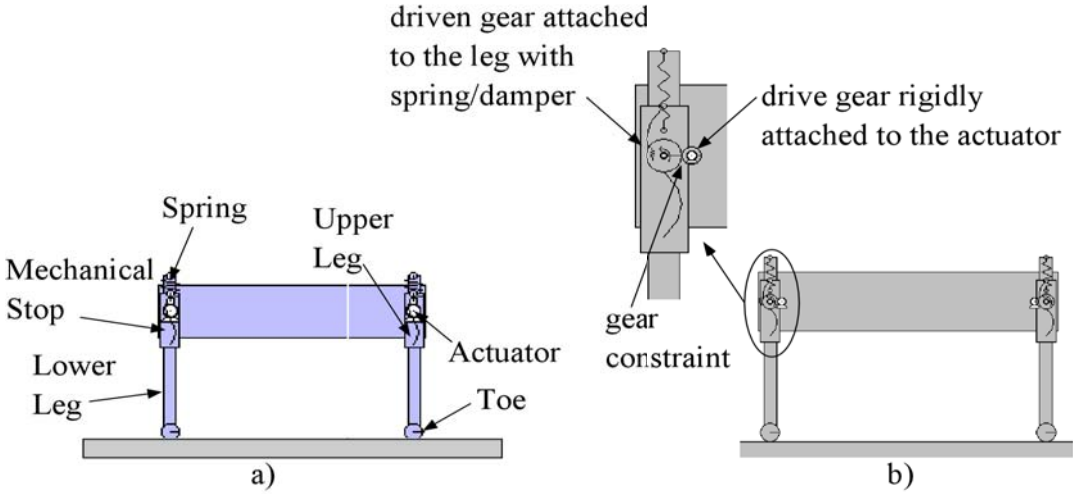

Figure 11. Scout II sagittal plane model built in Working Model™ 2D [18]: (a) *Model I* and (b) *Model II*.

Model I. In the simplest simulation model, called *Model I* (see Fig. 11a), the legs are attached to the body via an actuator constraint, which applies the torque to the leg, as calculated from the model described in Section 4.1. This model does not include the dynamics induced by the transmission mechanisms such as the gears and pulleys. This assumption has been widely used in analytical models for studying the basic properties of running (e.g. [9], [15], [34]), but, as will be shown in the following sections, it results in relatively large errors between simulation and experimental data in the case where compliant belts are present.

Model II. In the full model, called *Model II* (see Fig 11b), the hip unit has been modeled in more detail, as shown in Section 4.2. The leg is attached to the driven gear via a rotational

spring/damper system and the driven gear is attached to the drive gear via a "gear constraint" implementing the combined gear ratio of the gearbox and belt and pulley pair.

Table VI. Basic Mechanical Properties of Scout II

Parameter	Value	Units
Body Mass	20.865	kg
Body Inertia	1.3	kg m^2
Leg Mass	0.97	kg
Leg Inertia	0.01	kg
Spring Constant	3520	N/m
Damping Constant	55	N/m/s
Hip Separation	0.552	m
Leg Length	0.323	m

5.2. Simulation and Experimental Results

In this section the comparison between simulation and experimental data is undertaken. The controller gains and set points in simulation are the *same* as those used in the experiments and are presented in Table IV. In presenting the data, as with Muybridge [24], the term *step* refers to the stance phase together with the subsequent flight phase of one of the legs and the term *stride* refers to the combination of all four phases starting with the lift-off event of the back virtual leg, which is considered to be the reference leg. Therefore, for the sake of clarity, the body state variables are presented in detail for one stride while the leg variables and hip torques are presented for only one step.

Fig. 12 shows the pitch angle (left) and COM height (right) in experiment and in both simulation models corresponding to the highlighted region in Fig. 6. In experiment the pitch and COM hopping height are measured using two laser range finders located at the front and back ends of the body. The laser data were low-pass filtered after-the-fact at 15 Hz via FFT analysis in Matlab™ [20]. Unfortunately, as can be seen from Fig. 12, the remarkable match in the pitch angle did not extend to the hopping height where the difference between simulation and experiment, especially in *Model I*, is significant. This is attributed to the stiction and nonlinear damping (which depends on the leg angle and applied torque) effects that are inherent in the telescopic leg design and are not included in the simulation model. The difference in shape

results from the fact that the evolution of the COM height depends on both translation and rotation of the body that are strongly affected by the leg state sequence, which is slightly different between experiment and simulation. In experiment, front touchdown occurs slightly after back lift-off while in simulation it occurs slightly before.

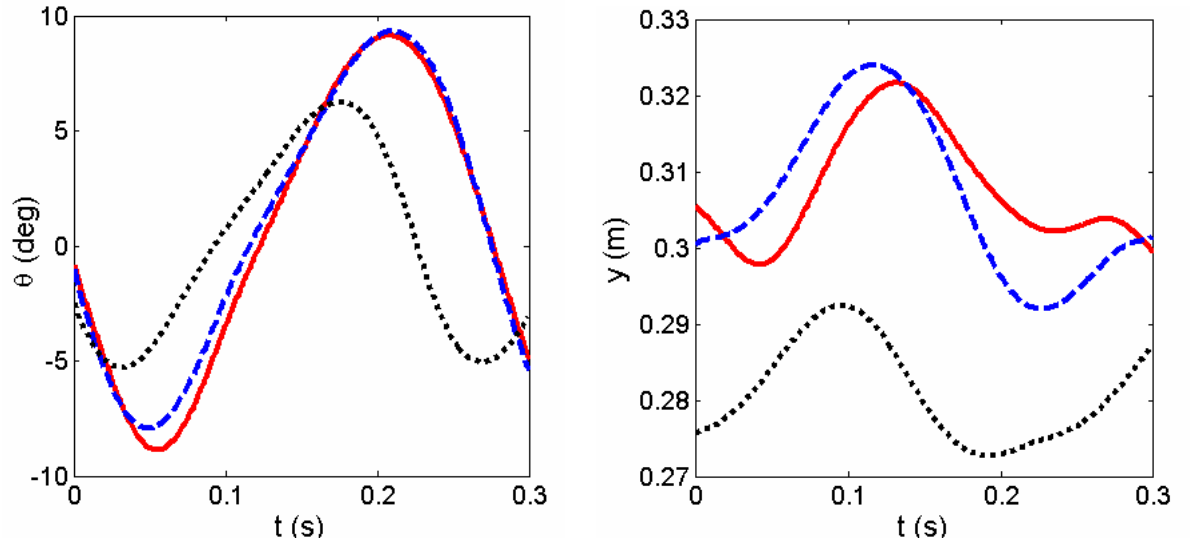

Figure 12. Steady state pitch angle (left) and COM height (right) during one stride. Experiment (solid), Model I (dotted) and Model II (dashed).

Fig. 13 shows the angles and angular velocities of the front and back legs relative to the body. For clarity, back and front leg plots correspond to one step and are synchronized based on the corresponding lift-off events. The square wave included in all the plots presenting data related to the legs represents the leg states: flight (high), stance-retraction (low) and stance-brake (medium). As expected, the leg response during the flight phase is significantly improved by the addition of the gearbox dynamics in *Model II*. Also, it is obvious from Fig. 13 that in the stance-retraction and stance-brake phases of both the front and back virtual legs the discrepancy between experimental and simulation results is larger than that of the flight phase.

The main source of errors in both models is the absence of a good estimate of the toe-ground friction coefficient combined with the simplifying assumptions in modeling the hip joint. However, including the hip model described in Section 4.2 significantly improves the accuracy of the simulation during the stance-brake phase. This is especially evident in the behavior of the back legs. For instance, in *Model I* the sweep limit controller is not able to hold the back leg at the desired sweep limit angle. This fact significantly affects the simulation results to the point

where cyclic motion might not even be achievable with the set points and gains used in experiment. This was the case in [38], where in simulation different sweep limit angles were used than those in experiment, for the model to converge in cyclic bounding motion.

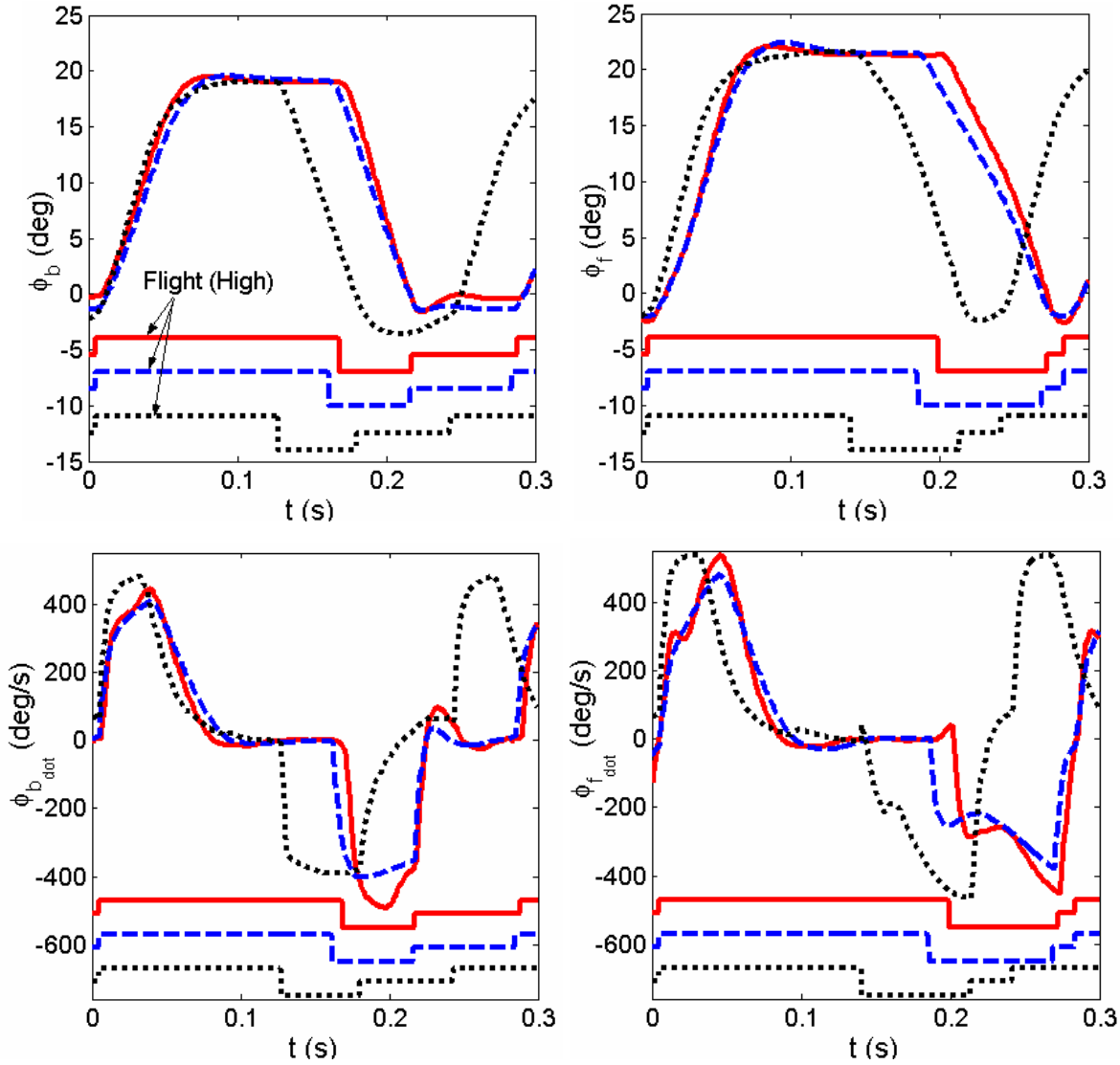

Figure 13. Back (left) and front (right) leg angles (upper) and leg angular velocities (lower) during one step. Experimental data (solid), Model I (dotted) and Model II (dashed) during one step. The square wave represents the leg states: Flight (high), stance-retraction (low) and stance-brake (medium).

It should be noted here that the stance-brake phase is very difficult to model in an accurate way because it depends on the interaction of several effects, which are difficult to estimate. In experiment, when the sweep limit is reached the motor initially loads the torsional

leg-belt-gear compliance without actually *feeling* the full load of the robot. Then, depending on the ground friction *and* the lift-off time instant (which itself depends on the robot's state), slipping might be present or contact with the ground might be lost. Thus, in experiment, it is *easier* for the motor to hold the leg at the desired angle during the stance-brake phase than in *Model I*, a fact that is adequately captured only by *Model II*.

Fig. 14 presents the torques applied by the motors in experiment and in simulation. As expected, there are relatively large discrepancies between the torques predicted by *Model I* and the torques estimated in experiment. In *Model II*, the simulation predicted torques are much closer to the current-estimated torques in experiment. However, it is clear that there are still discrepancies between experimental and simulation torques. These differences are coupled to the differences observed in the leg angle rates in Fig. 13, since motor saturation and thus torque application depends on the leg speed. This becomes apparent when one compares the torques in Fig. 14 with those predicted by the models, given in Fig. 9. Although the same motor model (14) has been used in both cases, the torques presented in Fig. 9 are much closer to the actual ones because they have been calculated using the encoder-measured motor shaft angular speeds during an experiment. On the contrary, the torques presented in Fig. 14 have been obtained using the simulation rotational speeds.

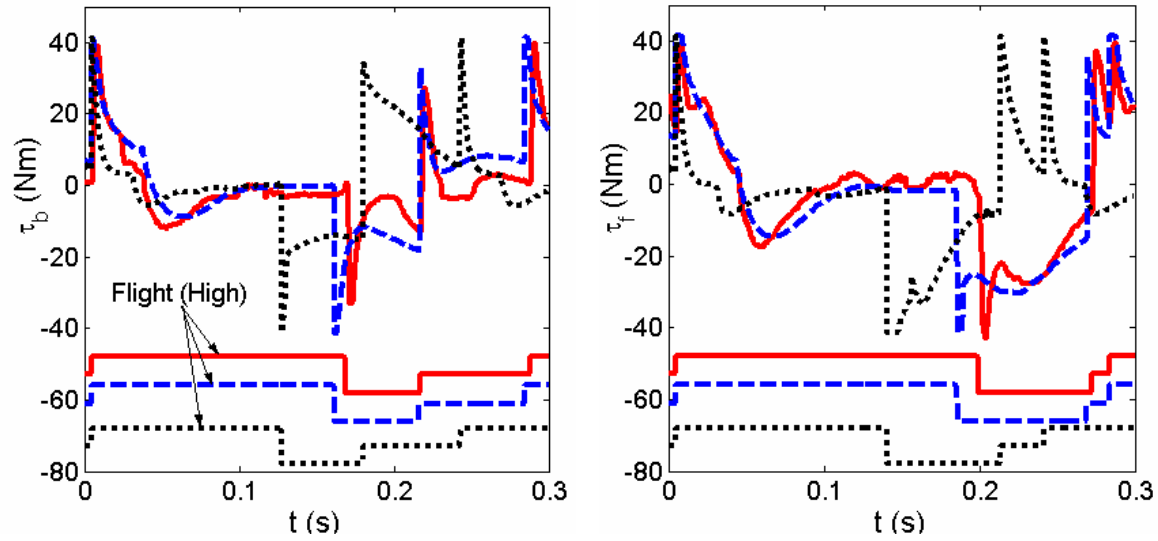

Figure 14. Back (left) and front (right) torques. Experimental data (solid), Model I (dotted) and Model II (dashed) during one step. The square wave represents the leg states: Flight (high), stance-retraction (low) and stance-brake (medium).

Fig. 15 shows the legs' angular speed as a function of the applied motor torque in experiment and simulation. The concentration of data points along straight lines (the motor's torque/speed line) in the first and third quadrants indicates that that the motors are saturated most of the time. As can be seen, both simulation models adequately capture this effect. Careful inspection of Fig. 15 reveals that most of the discrepancies lie in the non-saturation region, where the applied torques mostly depend on the dynamics of the system. Note also that according to the sign conventions shown in Fig. 3 during stance-retraction, the motors operate in the third quadrant while during flight they operate in the first quadrant (positive torques correspond to the leg moving forward), see Fig. 15.

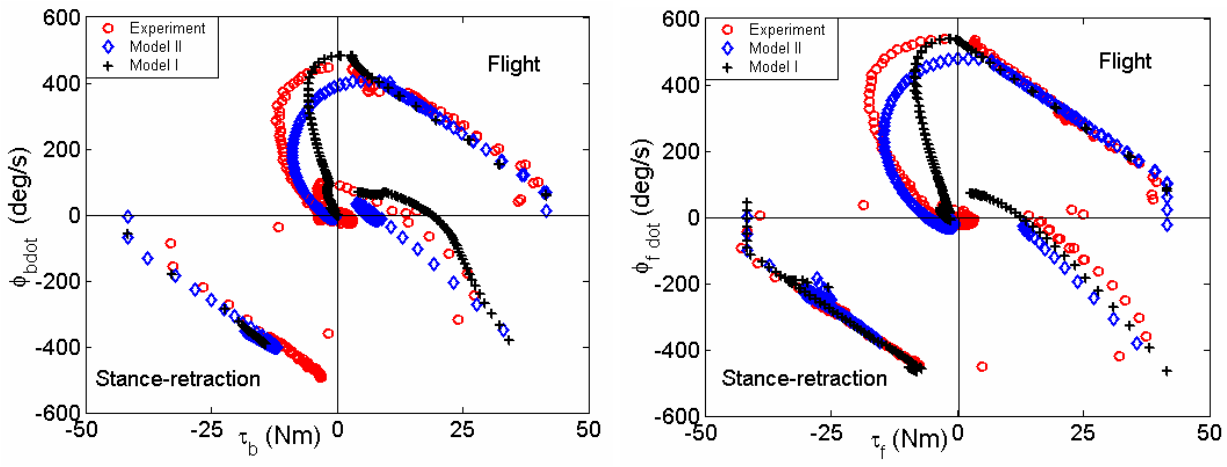

Figure 15. Back (left) and front (right) motor saturation characteristics.

5.3. Simulation Error Assessment

In this section an attempt is made to assess the quality of the simulation results obtained using the simulation models described in Sections 5.1 and 5.2. To do so, the results presented above for one stride have been generalized to multiple strides corresponding to different bounding experiments. Thus, for the comparison ten bounding experiments were performed on carpet. In each experiment, the robot took at least seven steady state strides defined by the back leg lift-off event. Unfortunately, due to the absence of sensors for measuring instantaneous forward speed, only the average speed was calculated for each experimental run. The average forward speed measured in the ten bounding experiments was 1.26 ± 0.04 m/s while the forward speed in *Model I* was 1.56 m/s, and in *Model II* was 1.43 m/s. Although a discrepancy exists in both models with respect to the actual robot, *Model II* still provides a closer representation of the robot's speed.

It is important to point out that the existence of phase difference between simulation and experimental results precludes state variable error calculations with respect to time. Therefore, the comparison is undertaken in terms of percent errors in some key gait parameters i.e. stride frequency ω_s, duty factor β, and the max and min values of the body's pitch angle and hopping height over the 70 strides taken. Fig. 16 reports the mean $\bar{e}_X \pm \delta\bar{e}$ and maximum errors $e_X^{\max}$ for each of the compared variables $X \in \{\omega_s, \beta_b, \beta_f, \theta_{\max}, \theta_{\min}, y_{\max}, y_{\min}\}$.

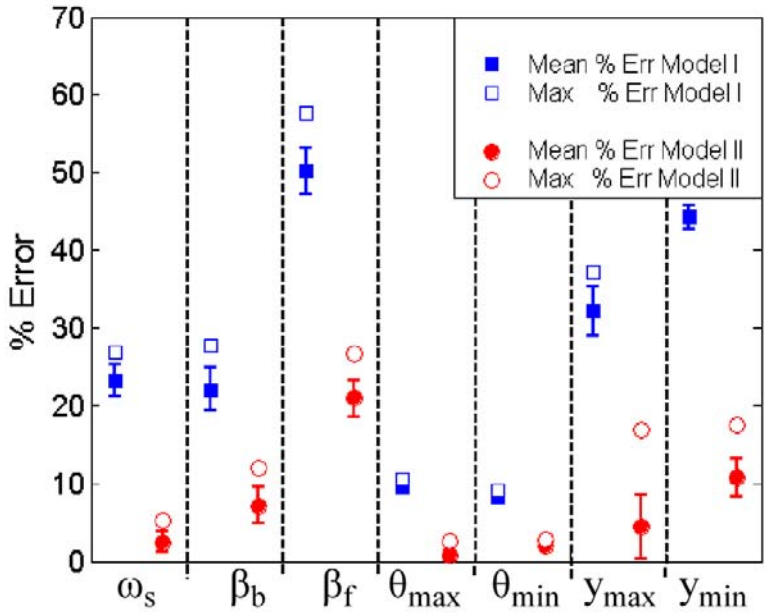

Figure 16. Mean and max errors between simulation models and experimental results in gait parameters and max and min values of the pitch and hopping height over 70 bounding strides at average forward speed approximately 1.3 m/s.

As can be seen from Fig. 16, despite the simplifying assumptions and the uncertainty associated with some of the design parameters, *Model II* captures the behavior of the robot not only qualitatively but also quantitatively. Indeed, the average errors for *Model II* in all the parameters are below the corresponding ones for *Model I*, and most strikingly, all are smaller than 25%, which is very good for dynamically stable robots. However, it is clear that there are still some issues that need to be resolved to provide a better match. For instance, the unmodeled gearbox efficiency varies as a function of the applied torque. In all the simulations the maximum gearbox efficiency was used to command and estimate torques since this is the only number available from the gear manufacturer. However, the gearbox efficiency varies dramatically as a

function of speed and torque, a fact that might explain some of the discrepancies between simulation and experiment. Maxon describes how the efficiency of the gearbox changes with the applied torque [21]. Unfortunately, this information is only qualitative and thus it has not been used in the simulation results presented here.

Despite the encouraging results of *Model II*, the exceptionally good match between simulation and experiment did not extend to average forward speeds drastically different from 1.3 m/s. In order to test the robustness of the models presented here, the authors repeated the experiments and simulations with controller set points that correspond to an average forward speed of approximately 0.8 m/s. At this speed, *Model I* (which already goes far beyond the modeling completeness common in the legged robot community) fails to bound entirely (the robot takes few steps and then stops). *Model II* still provides a very good estimate of the evolution of the individual variables (body pitch, leg angles, angular speeds and torques) but it converges to a "quasi-bounding" period-two gait, which bears a close resemblance to the bounding gait followed by the robot *but* repeats itself every two cycles. In one cycle, back leg lift-off occurs slightly *before* front leg touchdown while in the next cycle, back lift-off occurs slightly *after* front leg touchdown.

Nevertheless, this paper presented the first (to the authors' knowledge) thorough investigation of modeling issues for dynamically stable legged robots. It has been shown that assumptions common in modeling other types of robots cannot be transferred to dynamically stable legged robots, unless they are experimentally validated. Indeed, dynamically stable legged robots suffer from impacts, peak loads and a variety of control constraints not common in other robotic systems. Furthermore, absence of strong feedback control that would "push" the dynamics towards some *a priori* known desired trajectories, errors associated with the identification experiments, uncertainty in the knowledge of some parameters provided by manufacturers of certain components (e.g. dynamic gearbox efficiency), in combination with the intermittent nature of the system, are some of the qualities that make the task of obtaining an accurate simulation model challenging. However, establishing the role of modeling assumptions and the validity of the resulting models for dynamically stable legged robots is essential, both in identifying key properties inherent to system behavior and in achieving *prescriptive* models, which is the main reason for modeling.

6. CONCLUSION

This paper presented Scout II, a four-legged, untethered robot that runs in a dynamically stable fashion. Scout II relies on the passive dynamics of its mechanical system featuring a low degree of freedom actuation and passively compliant leg designs with only one actuator per leg. The authors proposed a very simple control algorithm that only relies on proprioceptive feedback from motor encoders and leg length potentiometers and results in running at average forward speeds up to approximately 1.3 m/s. Scout II provides an experimental instantiation of fundamental design and control principles for a new class of dynamically stable legged robots with reduced mechanical complexity and power requirements.

This paper also addressed a very important subject that has not received much attention in the dynamically stable legged robot literature: experimentally validated models. Two different simulation models were constructed to test the validity of commonly made assumptions in modeling dynamic legged robots. Both models included an experimentally validated motor driving system (amplifier/actuator units) with a battery model. Without the actuator saturation taken into account, both models do not converge to cyclic motion with the controller used in experiments.

The authors also demonstrated that in order to construct a model that accurately describes the physical behavior, one needs to include a detailed model of the hip joint including torsional belt compliance and gear dynamics. The assumption of rigid torque transmission is not valid and significantly affects the accuracy of the results. *Model I*, which already goes far beyond the modeling completeness common in the legged robot community but does not include torsional hip compliance, *not only* results in larger errors but, most importantly for lower speeds, fails entirely to converge to cyclic bounding motion. On the other hand *Model II* is remarkably accurate over a limited operating range. The authors hope that these results will shed light on which commonly made assumptions (e.g. constant maximum torque, rigid torque transmission) might result in misleading models especially for dynamic legged robots.

7. ACKNOWLEDGMENTS

We are indebted to Shervin Talebi, Martin de Lasa and Didier Papadopoulos who initiated and first implemented early versions of the bounding controllers described above, and to Geoff

Hawker, Robert Battaglia, Don Campbell and Dave McMordie for the design and construction of various parts of Scout II. Prof. Evangelos Papadopoulos and Prof. Inna Sharf provided useful comments. This project was supported in part by the Institute of Robotics and Intelligent Systems (IRIS, a Canadian Federal Network of Centers of Excellence) and the Natural Sciences and Engineering Research Council of Canada (NSERC). Ioannis Poulakakis has been supported by a R. H. Tomlinson Doctoral Fellowship and by the Greville Smith McGill Major Scholarship.

REFERENCES

[1] Advanced Motion Controls, *PWM Servo Amplifiers Catalog*, p. A-21, 1997. (http://www.a-m-c.com/ last accessed Nov. 21, 2003).

[2] Altendorfer R., Koditschek D., and Holmes P., "Stability Analysis of Legged Locomotion Models by Symmetry Factored Return Maps", in *Int. J. of Robotics Research*, Vol. 23, No. 11, pp. 979-1000, 2004.

[3] Battaglia R., *Design of the Scout II Quadruped with Preliminary Stair Climbing*, M.Eng. Thesis, McGill University, Montreal, QC, Canada, May 1999.

[4] Berkemeier M. D., "Modeling the Dynamics of Quadrupedal Running", in *Int. J. of Robotics Research*, Vol. 17, No. 9, pp. 971-985, 1998.

[5] Buehler M., Battaglia R., Cocosco A., Hawker G., Sarkis J., and Yamazaki K., "SCOUT: A Simple Quadruped that Walks, Climbs, and Runs," *Proc. of the IEEE Int. Conf. Robotics and Automation*, p. 1701-1712, Leuven, Belgium, May 1998.

[6] Buehler M., "Dynamic Locomotion with One, Four and Six-Legged Robots", in *J. of the Robotics Society of Japan*, Vol. 20, No. 3, pp. 15-20, 2002.

[7] Campbell D. and Buehler M., "Preliminary Bounding Experiments in a Dynamic Hexapod", *Experimental Robotics VIII*, in Springer Tracts in Advanced Robotics 5, B. Siciliano and P. Dario, (eds.), pp. 612-621, Springer-Verlag, 2003.

[8] de Lasa M. and Buehler M., "Dynamic Compliant Walking", *Proc of the IEEE Int. Conf. on Robotics and Automation*, pp. 3153-3158, Korea 2001.

[9] Formalsky A., Chevallereau C. and Perrin B., “On Ballistic Walking Locomotion of a Quadruped”, in *Int. J. of Robotics Research*, Vol. 19, No. 8, pp. 743-761, 2000.

[10] Freeman P. S. and Orin D. E., “Efficient Dynamic Simulation of a Quadruped Using a Decoupled Tree-Structure Approach”, in *Int. J. of Robotics Research*, Vol. 10, No. 6, pp. 619-627, 1991.

[11] Full R. J. and Koditschek D., “Templates and Anchors: Neuromechanical Hypotheses of Legged Locomotion on Land”, in *The J. of Experimental Biology*, Vol. 202, pp. 3325-3332, 1999.

[12] Furusho J., Sano A., Sakaguchi M. and Koizumi E., “Realization of Bounce Gait in a Quadruped Robot with Articular-joint-type Legs”, in *Proc of the IEEE Int. Conf. on Robotics and Automation*, pp. 697-702, Japan 1995.

[13] Gabrielli G. and von Karman T. H., “What Price Speed?”, *Mechanical Engineering*, Vol. 71, No. 10, 1950.

[14] Ghigliazza R. M., Altendorfer R., Holmes P. and Koditschek D. E., “Passively Stable Conservative Locomotion”, in *SIAM J. of Applied Dynamical Systems*, Vol. 2, No. 2, pp. 187-218, 2003.

[15] Herr H. M. and McMahon T. A., “A Galloping Horse Model”, in *Int. J. of Robotics Research*, Vol. 20, No. 1, pp. 26-37, 2001.

[16] Hirose S., “Super Mechano-System: New Perspective for Versatile Robotic System”, *Experimental Robotics VII*, in Lecture Notes in Control and Information Sciences 271, D. Rus and S. Singh (eds), Springer-Verlag, pp. 281-289, 2001.

[17] Kimura H., Akiyama S. and Sakurama K., "Realization of Dynamic Walking and Running of the Quadruped Using Neural Oscillator", *Autonomous Robots*, Vol.7, No.3, pp. 247-258, 1999.

[18] Knowledge Revolution, *Working Model 2D User’s Guide*, Version 5.0, San Mateo, CA, 1996. (http://www.krev.com last accessed Nov. 21, 2003).

[19] Kubow T. M. and Full R. J., "The Role of the Mechanical System in Control: A Hypothesis of Self-stabilization in Hexapedal Runners", in *Philosophical Trans. of the Royal Society of London Series B – Biological Sciences,* 354 (1385), pp. 854-862, 1999.

[20] MathWorks, *Matlab*, Ver. 6.1, Natick, MA, 1998. (http://www.mathworks.com/ last accessed Nov. 21, 2003).

[21] Maxon Motors AG, *Motor Catalog*, p. 77, 1997. (http://www.mpm.maxonmotor.com/ last accessed Nov. 21, 2003).

[22] McGeer T., "Passive Bipedal Running", *Technical Report, CSS–IS TR 89-02*, Simon Fraser University, Centre For Systems Science, Burnaby, BC, Canada, 1989.

[23] Moore E. Z., *Leg Design and Stair Climbing Control for the RHex Robotic Hexapod*, M.Eng. Thesis, McGill University, Montreal, QC, Canada, January 2002.

[24] Muybridge E., *Animals in Motion*, Dover Publications, New York, 1957.

[25] Nichol J. G. and Waldron K. J., "Biomimetic Leg Design for Untethered Quadruped Gallop", *Int. Conf. on Climbing and Walking Robots (CLAWAR)*, pp. 49-54, France, 2002.

[26] Papadopoulos D. and Buehler M., "Stable Running in a Quadruped Robot with Compliant Legs", *Proc. of the IEEE Int. Conf on Robotics and Automation*, pp. 444-449, U.S.A., 2000.

[27] Poulakakis I., *On the Passive Dynamics of Quadrupedal Running*, M.Eng. Thesis, McGill University, QC, Canada, July 2002.

[28] Poulakakis I., Papadopoulos E. and Buehler M., "On the Stable Passive Dynamics of Quadrupedal Running", *Proc of the IEEE Int. Conf. on Robotics and Automation,* pp. 1368-1373, Taiwan, 2003.

[29] Poulakakis I., Smith J. A., and Buehler M., "On the Dynamics of Bounding and Extensions Towards the Half-Bound and the Gallop Gaits", *Int. Symp. on Adaptive Motion of Animals and Machines*, Japan, 2003.

[30] Poulakakis I., Smith J. A., and Buehler M., "Experimentally Validated Bounding Models for the Scout II Quadruped Robot", *Proc. of the IEEE Int. Conf. on Robotics and Automation*, New Orleans, U.S.A, 2004.

[31] Raibert M. H., Brown Jr. H. B., Chepponis M., Hodgins J., Kroechling J., Miller J., Murphy K., N., Murthy S. S. and Stentz A., "Dynamically Stable Legged Locomotion", *Technical Report, CMU-LL-4-1985*, Carnegie Mellon University, The Robotics Institute, Pittsburgh, PA, U.S.A., Feb. 1985.

[32] Raibert M. H., *Legged Robots that Balance*, MIT Press, Cambridge MA, 1986.

[33] Saranli U., Buehler M., and Koditschek D. E., "RHex: A Simple and Highly Mobile Hexapod Robot", in *Int. J. Robotics Research*, Vol. 20, No. 7, pp. 616-631, 2001.

[34] Schmiedeler J. P. and Waldron K. J., "The Mechanics of Quadrupedal Galloping and the Future of Legged Vehicles", *Int. J. of Robotics Research*, Vol. 18, No. 12, pp. 1224-1234, 1999.

[35] Seyfarth A., Geyer H., Guenther M. and Blickhan R., "A Movement Criterion for Running", in *J. of Biomechanics*, Vol. 35, pp. 649-655, 2002.

[36] Song S. –M. and Waldron K. J., *Machines That Walk: The Adaptive Suspension Vehicle*, MIT Press, Cambridge MA, 1989.

[37] Talebi S., *Compliant Running and Step Climbing of the Scout II Platform*, M. Eng. Thesis, McGill University, Montreal, QC, Canada, November 2000.

[38] Talebi S., Poulakakis I., Papadopoulos E. and Buehler M., "Quadruped Robot Running with a Bounding Gait", *Experimental Robotics VII*, in Lecture Notes in Control and Information Sciences 271, D. Rus and S. Singh (eds), Springer-Verlag, pp. 281-289, 2001.

[39] Yamamoto Y., Fujita M., De Lasa M., Talebi S., Jewell D., Playter R. and Raibert M., "Development of Dynamic Locomotion for the Entertainment Robot – Teaching a New Dog Old Tricks, *4th Int. Conf. on Climbing and Walking Robots (CLAWAR)*, pp. 695-702, 2001.